Atmospheric Environment: X 3 (2019) 100037

Contents lists available at ScienceDirect

Atmospheric Environment: X

journal homepage: www.journals.elsevier.com/atmospheric-environment-x

First two and a half years of aerosol measurements with an AERONET sunphotometer at the Huancayo Observatory, Peru

René Estevan[a,*], Daniel Martínez-Castro[a,b], Luis Suarez-Salas[a], Aldo Moya[a], Yamina Silva[a]

[a] Instituto Geofísico del Perú, Lima, Peru
[b] Instituto de Meteorología, La Habana, Cuba

HIGHLIGHTS

- Characterization of the two and a half years of aerosol measurements at the Huancayo Observatory, Peru.
- Aerosol classification define six aerosols types for the location with the predominance of continental type.
- Aerosols background conditions predominate over measurement site, disrupted by the biomass burning season in south America.
- Biomass aerosols generated by neighboring countries such as Brazil and Bolivia, are transported to Huancayo.

ARTICLE INFO

Keywords:
AOD
AERONET
Huancayo observatory
Optical properties
Single scattering albedo
Asymmetry factor

ABSTRACT:

Direct sun measurements with a CIMEL sunphotometer belonging to the AERONET network have been performed in the Huancayo Observatory, Peru, from March 2015 to August 2017, two and a half years, providing for the first time information about aerosols in the specific area. The prevalence of background conditions in the measurement site has been determined for the period of study. These conditions, which constitute more than 80% of cases, are occasionally altered, mainly by high aerosols loading, as a consequence of biomass-burning events. Biomass-burning periods cover every year from mid-July to mid-October. The identification of these periods has been possible through the classification of aerosols in 6 subtypes. The month with the maximum AOD monthly average is September, and in 2016, the absolute maximum value of 0.91 was registered. The mean AOD value for the study period is 0.10 ± 0.07 and the alpha mean value is 1.49 ± 0.36, indicating presence, of small size aerosols. Some aerosol optical properties were analyzed in order to validate the aerosol classification. The aerosol size distribution revealed a bimodal character with a slight predominance of the fine mode, related to the two main types of aerosols: continental and biomass.

1. Introduction

Aerosols have a direct and indirect effect on both weather and climate, because of their direct and indirect effects (IPCC, 2007). At present, much knowledge has been gained about the characteristics and properties of aerosols and, as a result, the uncertainty about their effects on weather and climate has been considerably reduced (IPCC, 2013). This has been achieved largely due to the increases measurements from satellite, aerial platforms and ground stations. However, for a better understanding of aerosols' physical and optical properties, extensive ground-based measurements are still required (Alados-Arboledas et al., 2008). Ground radiometric measurements offer key information which complements that provided by satellites. A successful example of surface aerosol measurements is the global sunphotometer network AERONET, coordinated by NASA (Holben et al., 1998). Since the network was created it has aimed at monitoring the aerosol worldwide in order to establish a long-term global aerosol climatology. The validation of satellite-based aerosol measurements has been another of its goals (Holben et al., 2001).

Mountain ecosystems, especially the glaciers with altitudes above 4000 m above sea level (masl) in the tropical regions, are very sensitive to climate change (Chevalier et al., 2011). Black carbon and other light absorbing pollutants deposited over the glacier snow reduce the snow albedo (Warren and Wiscombe, 1980; Jacobson, 2004) and, consequently, produce snow melting (Warren, 1984). The South American Andes mountain chain dominates the western side of South America, extending to seven countries in the continent and constituting a natural barrier to the easterly trade winds from the Atlantic Ocean. According

* Corresponding author.
E-mail address: restevan@igp.gob.pe (R. Estevan).

https://doi.org/10.1016/j.aeaoa.2019.100037
Received 24 October 2018; Received in revised form 20 May 2019; Accepted 25 May 2019
Available online 20 June 2019

to Dyurgerov and Meier (2005), the Central Andes, where part of Peru is located, contain more than 99% of the world's glaciers in tropical latitudes, with Peru accounting for 70% of this amount. Black carbon, which is a strongly absorbing component of carbonaceous aerosols, have an important effect on snow reflectance (Warren and Wiscombe, 1980). It has a direct effect on snow radiative forcing, which is three times more than CO2 forcing (Flanner et al., 2007).

Biomass-burning is one of the most important sources of black carbon aerosols, and in South America, the Amazon basin is the main source of this type of aerosols (Mishra et al., 2015). Every year, at the southern hemisphere, large amounts of smoke can be observed from the space between August and November (Andreae, 1993). This large aerosol loading seriously affects not only the Andes cryosphere and the air quality but also human health (De Oliveira Alves et al., 2017). Land use changes in the Amazonia cause alterations of many atmospheric properties, and these changes significantly affect the Amazonian ecosystem (Artaxo et al., 2013). This study aims to determine if the biomass aerosols generated by the biomass burning fires in the Amazon reach the central Andes where the HYO is located and to know the extent to which Aerosol Optical Depth (AOD) affects this site.

The only AERONET sunphotometer that has been operating continuously in Peru for atmospheric aerosols measurements is installed at the Huancayo Observatory (HYO), located at 12.04° S and 75.32° W at an altitude of 3313.0 masl. Continuous measurements of AOD and other aerosol optical properties began on March 19, 2015, and has extended, uninterrupted, to the present. The studies about atmospheric aerosols in the Mantaro Valley are very scarce and have been based on satellite information, specifically the Moderate Resolution Imaging Spectroradiometer (MODIS), Total Ozone Mapping Spectrometer (TOMS) (Suárez et al., 2006) and MODIS and Ozone Monitoring Instrument (OMI) (Vivanco, 2014). In both cases, it has been found that, the highest AOD values are recorded between the middle and late winter and early and mid-spring. The contribution to the aerosol loading in HYO, from biomass-burning fires both in Peru and in neighboring countries, has been addressed using satellite information (Suárez et al., 2006) and through numerical modeling (Moya et al., 2017). The lack of ground-based measurement studies on atmospheric aerosols in Peru, and particularly in the Mantaro Valley, has been the main motivation for the development of this study. The absence of investigations on atmospheric aerosols using surface instruments has been another motivation. Consequently, the objective of the present work is the characterization and classification of atmospheric aerosols measured in HYO in two and a half years by means of a sunphotometer.

2. Site, instrument and data

Measurement site

Aerosol measurements are carried out in the Laboratory of Atmospheric Microphysics and Radiation (LAMAR, in Spanish). The lab, which belongs to the Geophysical Institute of Peru (IGP, for its acronym in Spanish), is also part of the HYO. The observatory is located in the Central Peruvian Andes inside the valley formed by the Mantaro River (Fig. 1), which is part of the Department of Junín, Peru. It is located in a rural environment and surrounded by non-irrigated farmlands, approximately 12 km westward of Huancayo City, which is the largest city in the central Peruvian Andes with a population of more than 400 000 inhabitants. This is a growing city, with an increasing adoption of automotive parks and other pollution sources.

Instrument and dataset

The instrument used for aerosol measurements is the sunphotometer CIMEL CE-318T. It was installed on March 19, 2015, as part of the AERONET network. Besides being the only instrument of this type in Peru, it is also the only remote ground-based detection point for aerosol measurements in the country.

To date, three of these instruments have been used in HYO, as shown in Table 1. Up to August 31, 2017, a total of 878 days of measurements have been made in Level 1.0, and this is the level to which the raw data correspond. At Level 1.5 correspond 854 days (97.3%); the data in this level is not quality assured, but it is cloud screened (Smirnov et al., 2000). Pre- and post-field calibration is applied to the maximum quality assured level (Level 2.0), and the data is automatically cloud cleared and manually inspected. To this level correspond a total of 737 days (83.9%). For this study, the dataset corresponding to the maximum quality level will be used. All these instruments have been calibrated and post-calibrated in the facilities of AERONET GSFC in NASA to guarantee the accuracy and reliability of the data.

The CIMEL CE-318T uses eight spectral bands for solar and sky irradiance measurements (340, 380, 440, 500, 675, 870, 1020 and 1640 nm). Direct sun measurement, known as the SUN scenario, is the common procedure of the sunphotometer for aerosol measurements. With a frequency of 15 min, this scenario is used to retrieve the spectral Aerosol Optical Depth (AOD) and the Angström Exponent (Eck et al., 1999). The Almucantar and Principal Plane scenarios are used for the sky irradiance measurements from which various aerosol properties are retrieved using inversion methods. Some of these properties are aerosol sizes distribution, single scattering albedo, extinction coefficient, etc. (Dubovik and King, 2000; Dubovik et al., 2006).

The AOD at 440 nm and the Angström Exponent (α), in the range of 440–870 nm, will be the main variables for this study. The Angström Exponent is commonly used as a good indicator of the atmospheric particles' size (Dubovik et al., 2002). Normally, values of $\alpha < 0.5$ imply the predominance of large particles, also known as coarse mode; on the other hand, values of $\alpha > 1.5$ imply the predominance of very small particles and aerosols located on this side of the size distribution, also known as the fine mode. The combination of these two variables will be used for aerosol classification.

As aerosol microphysical properties, we will analyze the aerosol volume-size distribution, single scattering albedo (SSA) and asymmetry factor (AF, commonly represented by the letter g) across four wavelengths (440, 675, 870, 1020 nm). These properties will be basically used to validate or corroborate the aerosol classification. The temporal resolution of this information is very low and the difficulty is determined based on sky condition requirements. Clear sky conditions, large scattering angles (larger than 50°) and values of AOD > 0.4 are necessary to derive these magnitudes (Holben et al., 2006). For this reason, only 16 cases are available with SSA measurements, where 10 correspond to July 2016 and the rest to September, the month with maximum AOD values due to the biomass-burning. Within these September cases, 3 measurements correspond to the ones in year 2015 and 3 to the ones in 2016. In the case of AF, 538 measurements have been made. All the variables used in the present study correspond to the period covered from March 19, 2015, to August 31, 2017, and are classified as Level 2.0 of AERONET.

Air masses and synoptic conditions

The main synoptic circulation in Peru corresponds to a well-marked anticyclonic circulation at high levels of the troposphere, centered in Bolivia and known as the Bolivian high (Lenters and Cook, 1997). This anticyclonic circulation guarantees strong divergence in high levels over a large part of Peru. According to Silva et al. (2008), two main seasons, the rainy and the dry season occur in Peru, in general, and in the Mantaro Valley, in particular. Rainfall in Peru is concentrated in the period between September and April, while very little rainfall occurs in the period between May to August, so a marked seasonality is present in the region (Aceituno, 1989; Vuille et al., 2008; Garreaud, 2009). During the dry period, the high-level anticyclonic circulation center is removed from Bolivia and, in consequence, the divergence in Peru decreases

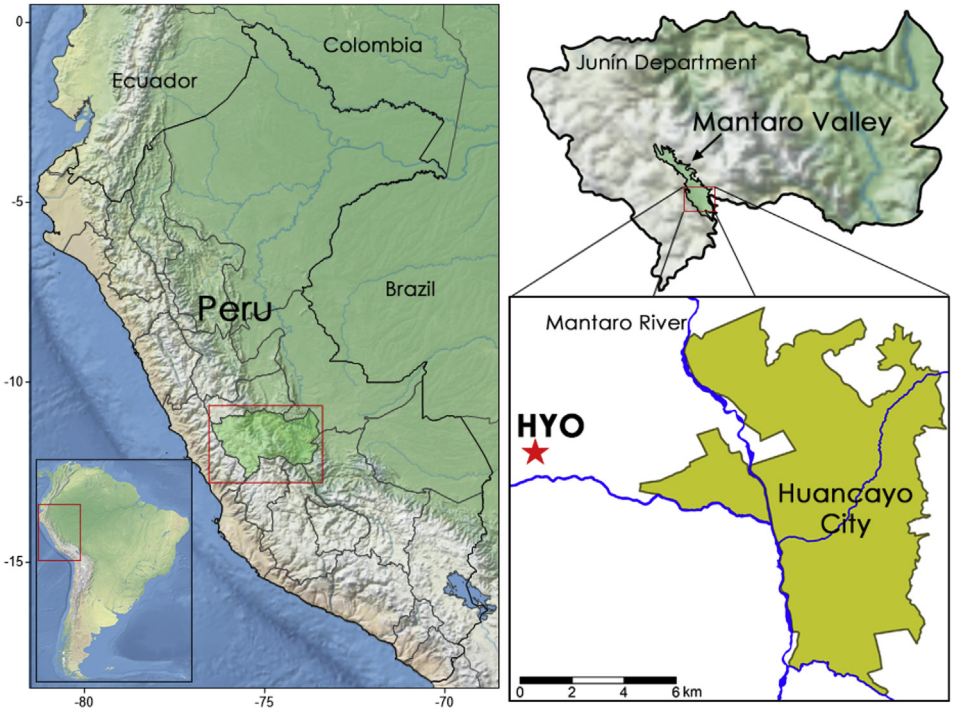

Fig. 1. The measurement site is located at Laboratory of Atmospheric Microphysical and Radiation in the HYO, belonging to the IGP. The observatory is inside the Mantaro Valley, at the Central Peruvian Andes, Junín department, Peru.

Table 1
Sunphotometers, with the corresponding AERONET number, used at HYO.

Instrument	Start Date	End Date	Number of Days	Quality Level
#890	03/19/2015	06/21/2016	448	2.0
#929	06/22/2016	08/31/2017	429	2.0
#923	09/30/2017	present	counting	1.5

markedly while the eastern humid flow is weakened at medium levels, giving rise to a stable and dry climate in the central Andes. During the rainy period, the moist air of the middle troposphere, coming from the Amazon, flows over the Central Andes and converges in the afternoon with the mountain-valley circulation. This flow is responsible for the occurrence of convective summer storms in this region (Garreaud, 1999; Vuille, 1999; Vuille et al., 2000; Garreaud et al., 2003; Vuille and Keimig, 2004).

To investigate the possible origin of the air masses that contribute to the presence of aerosols over HYO, a monthly back trajectory analysis was carried out at the surface level. For this purpose, NCEP/NCAR reanalysis (Kalnay et al., 1996) was conducted between January 2015 and December 2018. The trajectories for each month, of each year involved, have been calculated using a time step of 6 h and a duration of 120 h backwards. The origin point was located in HYO at the surface level. Finally, the trajectories were grouped by months and divided into eight different wind directions (Fig. 2). The prevalence of the north direction (N) is evident from its 51.6%, and that is followed by the northeast direction (NE) (19.5%). Considering the whole sample, 71.1% of all the trajectories reaching HYO arrived between N and NE. Particularly between April and September, this percentage always exceeded 80%, with the maximum frequencies in July and August with 94.9 and 94.7%, respectively.

Two main patterns can be considered from Fig. 2, with two transition months (April and September). In the first pattern, including the first and last trimesters (January to March and October to December), the trajectories show similar characteristics, with the predominance of N and NE winds directions, but also with the important contribution from south (S) and southwest (SW) directions. However, in the last trimester, the frequencies from S and SW are less than in the first trimester, and the influence from NW is greater.

As an example of this pattern, Fig. 3a shows all the trajectories calculated for the months of February in the three years involved. As can be seen in this figure, trajectories from S and SW flow over the Pacific Ocean, cross over the coastal Peruvian deserts and reach HYO. These kind of trajectories can drag dust particles from the coastal desert (Platero et al., 2018). On the other hand, winds from the north and northeast flow over the continent all the time.

During April, the first of the two transition months considered here (Fig. 3b), the frequencies of the trajectories from S and SW, which flow over the ocean, are considerably less. The second pattern includes the months from May to August, where the dominance of the N and NE winds at the surface is almost absolute. It is significant to note that there are no trajectories over the ocean during these months, so the particles move over the continent all the time. July is the most representative month of this second pattern and, as can be seen in Fig. 3c, the trajectories in the sectors from N to NE, in addition to some trajectories that originate in the E, are very concentrated. The trajectories that make up this pattern flow through a large part of the Central Peruvian Amazon and, in some cases, from Brazil, during a period in which a large number of biomass-burning fires occur.

September is the second month considered as the transition between the two patterns (Fig. 3). With the predominance of N direction trajectories and, therefore, with the characteristics of continental air masses, some trajectories originating in the ocean begin to appear again. The presence of trajectories originating in Brazil and carrying aerosols generated by the biomass-burning in the Brazilian Amazon can also be noticed.

3. Results

The daily average values (blue dots) with the respective standard deviations of AOD (top) and alpha (bottom), for the period between March 19, 2015, and August 31, 2017, are shown in Fig. 4. The

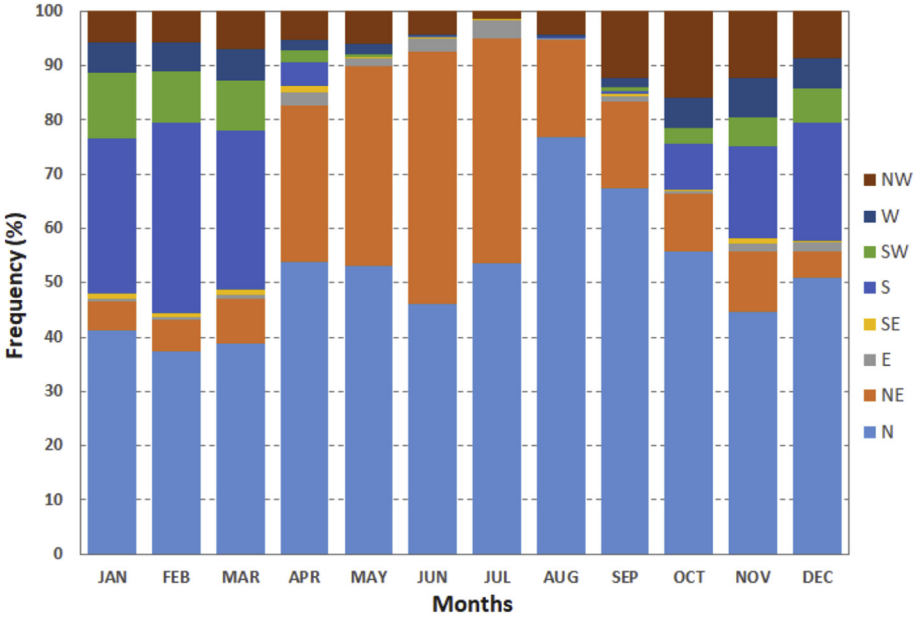

Fig. 2. Monthly frequency of wind directions derived from back trajectory analysis. Eight directions were considered: North (N), Northeast (NE), East (E), Southeast (SE), South (S), Southwest (SW), West (W) and Northwest (NW).

biomass-burning seasons for each year are shaded in light gray. The mean value of AOD for the period is 0.102, with a standard deviation (σ) of 0.066, obtained from all the instantaneous measurements during the period. This AOD value is related to low concentrations of atmospheric aerosols; however, the maximum average daily value is 0.492 and corresponds to September 14, 2016. The large values of AOD standard deviations during the biomass-burning seasons are indicative of large variability, which suggests that the arrival of biomass-burning aerosols (BIO) to HYO occurs during sporadic events rather than continuously. This result is very similar to those found in studies of other high mountain sites such as La Paz (Pérez-Ramírez et al., 2017) and the Himalayas (Dumka et al., 2008).

An increase in the average daily values was noticeable between the end of July and the beginning of October, for the years 2015 and 2016. This increase is likely related to biomass-burning, as discussed below. Other AOD high values are mainly related to isolated events of biomass-burning, outside the range of months mentioned above. Since July 2017, an AOD increasing trend, related to the beginning of the biomass-burning season for this year, has remarkably been noticed.

In the case of alpha, the mean value is 1.49 ± 0.36, which refers to the prevalence, on average, of small particles. However, the presence of low alpha values, which are related to large particles, is notable around February 2016 and between April and May 2016. The low alpha values are mainly related to maritime and dust aerosols. This can be corroborated with the trajectories shown in Fig. 3a corresponding to February, according to which 53% of trajectories originate in the ocean and cross the Peruvian coastal deserts before reaching HYO. These trajectories, when crossing the coastal deserts at ground level, can drag dust particles suspended in the air due to strong winds such as the "Paracas wind" (Escobar, 1993; Quijano, 2013; Briceño-Zuluaga et al., 2017), which takes its name from the homonymous peninsula. On the other hand, the existence of high values of alpha ($\alpha > 2.0$), during December 2015 and between February and May 2016, correspond to very small particles that can be related to anthropogenic aerosols associated with urban environments.

The AOD and Angström Exponent monthly climatology and related statistics, based on instantaneous measurements, are shown in Fig. 5. The box plots represent the range between the 25th and 75th percentiles, with the in-box dot showing the monthly mean value. The median is represented by the red line within the box, and the upper and lower whiskers extend to the most extreme data points that are not considered outliers. The AOD monthly mean values except for the period between July and October, which is related to the biomass-burning season as mentioned above, are below 0.1. The median exceeds the 0.1 value only for August and September. Since June, with the onset of winter and, therefore, the driest period of the year, there is an increase in the AOD values, with it beginning to reach the maximum value (0.164 ± 0.093) in September. This is also the month with the highest alpha value (Fig. 5b), with a magnitude of 1.75 ± 0.21. The large number of outliers is remarkable in the AOD, especially for July and September, which can be an indication of the diversity and high number of aerosols events. With respect to alpha, September is also the month with maximum value $\alpha = 1.75$ and the month with lower standard deviation (0.21). The highest mean alpha values occur between August and October, in addition to December. From June to October, no cases with alpha higher than 2.2 are found, with most outliers corresponding to very low alpha values (coarse mode).

The lowest average monthly values of AOD (AOD < 0.07) occur between January and May where the AOD remains stable around 0.065, except in February. January and February, followed by March, are the months with maximum rainfall in HYO. February is the last month of the summer season in the southern hemisphere, and its relative high AOD value (0.096), with respect to the rest of the wet season months, is associated with the biomass-burning and dust aerosols events explained above. However, the BIO type, which occurs in this month, must be related to the burning of crop residues that take place in the farmland surrounding the observatory.

April and May, the last two months of the fall season, have the lowest AOD monthly mean values (0.063 ± 0.031 and 0.064 ± 0.025, respectively). The lowest monthly mean alpha value (1.34 ± 0.35) corresponds to May (Fig. 5b). These high values are related to the biomass-burning season. The lowest monthly mean value of alpha also took place on May with a value of 1.34; however, a high number of outliers are present. This is the only month without the presence of BIO type. Table 2 shows the period statistics for both AOD (440 nm) and alpha (440–870 nm). The differences between the mean and median stand out in this table. In the case of AOD, the mean value is greater than the median, and in the case of alpha, the opposite is true.

Fig. 6 represents the relative frequencies distribution for both variables, AOD and alpha, corresponding to all the registered cases

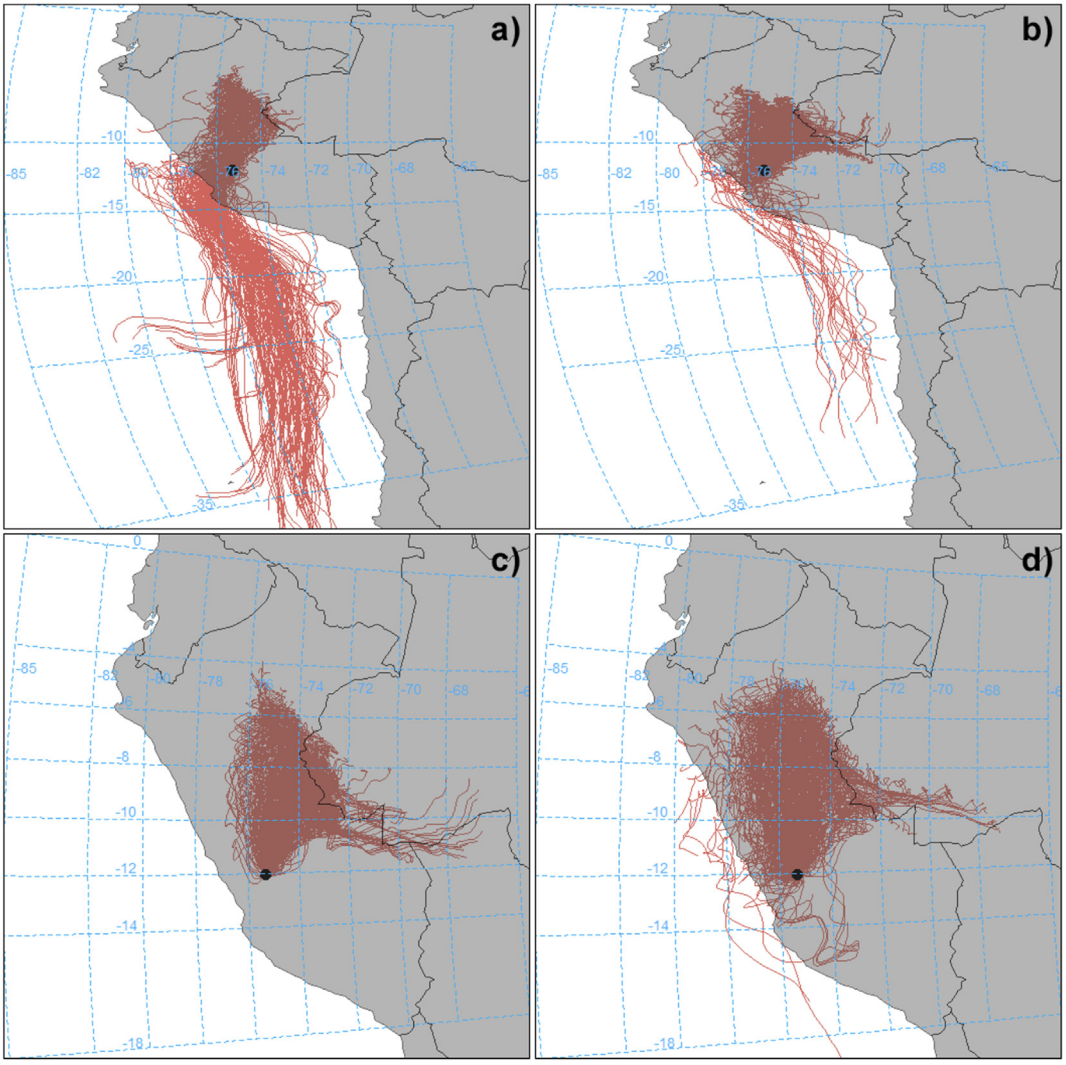

Fig. 3. Trajectories calculated for each month including the three years (2015–2017). February (a) and July (c) are the most representative months of the two patterns. April (b) and September (d) represent the transition months. All trajectories were calculated with an interval of 6 h and 120 h backwards at ground level. The black dot represents the HYO.

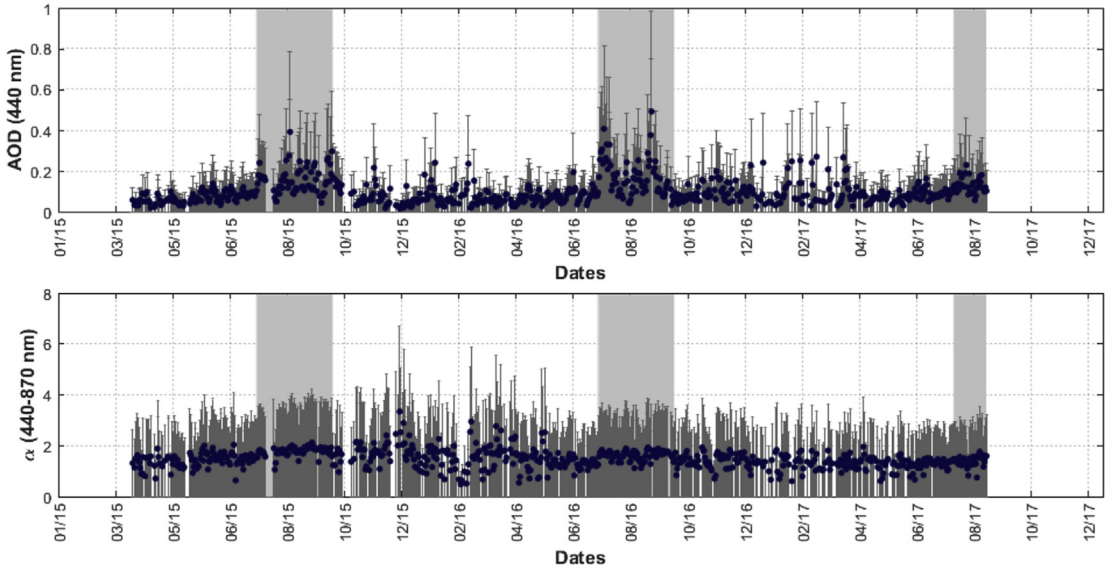

Fig. 4. Daily mean values and standard deviations for AOD at wavelength of 440 nm (top) and Angström Exponent (α) in the range of 440–870 nm (bottom) for the period 2015–2017. Shaded areas in light gray correspond to the biomass-burning seasons of each year.

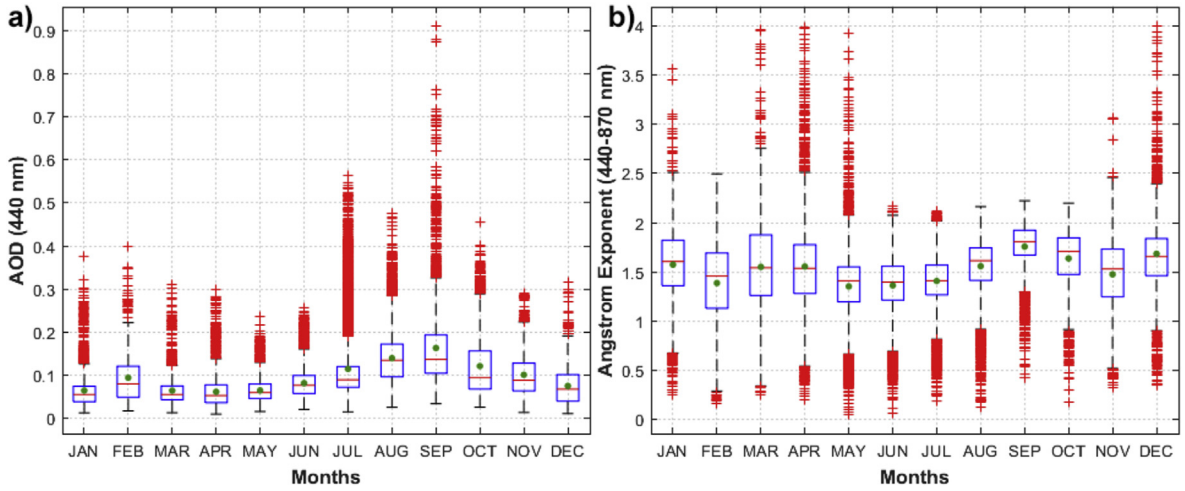

Fig. 5. Monthly climatology and the associated statistics for AOD (a) and alpha (b) during the study period. The monthly mean values are represented in plots with a green point within a rectangle and the red horizontal line segment represents the median. The top and bottom rectangle limits represent the 75th and 25th percentile, respectively and the red plus sing represents the outliers. (For interpretation of the references to color in this figure legend, the reader is referred to the Web version of this article.)

Table 2
General statistics for AOD (440 nm) and alpha (440–870 nm) for the analyzed period.

N = 50253	Average	STD	Max	Min	Median
AOD	0.102	0.066	0.91	0.01	0.085
alpha	1.49	0.36	3.99	0.06	1.51

(50253) during the study period. The highest frequency in the case of AOD corresponds to a value of 0.08 with 29.9%, followed by the value of 0.048 (25.2%). Of the total cases, 55.1% are concentrated between these two values. The values of AOD < 0.1 reach a total of 59.5%, which indicates the prevalence of background conditions for the measurement site. In third place of occurrence frequency is the value of AOD = 0.112 with a 17.5%, followed by the value of 0.144 (8.9%). Both values add up to 26.4%. If all the cases with AOD ≤0.144 are grouped, they constitute 85.9% of the whole sample, so the predominance of background conditions over the measurement site is evident. The rest of the cases (14.1%) with AOD higher than this magnitude is associated with pollution events such as the biomass-burning and dust aerosols.

The magnitude of the highest frequency of occurrence for the Angström Exponent corresponds to the value 1.470, in 17.8% of cases. Within the range of values $1 < \alpha \leq 1.75$, 78% of cases are concentrated, which implies the prevalence of aerosols of small size generally associated with aerosols of continental origin. Below the unit, we found that 7.5% of cases are associated with larger aerosols related to dust particles and maritime aerosols. The 14.2% of cases were found for $\alpha > 1.8$, very small particles.

Aerosols classification

There are several methods for aerosols classification (Hess et al., 1998; Dubovik et al., 2002; Gobbi et al., 2007; Russell et al., 2010). However, the most commonly used is the construction of an AOD versus alpha scattergram (D'Almeida et al., 1991; Eck et al., 1999; Holben et al., 2001; Vergaz et al., 2005; Otero et al., 2006; Toledano et al., 2007; Verma et al., 2015), where the AOD provides information on the aerosol loading and alpha about their sizes. The joint analysis of these two variables allows a better data interpretation.

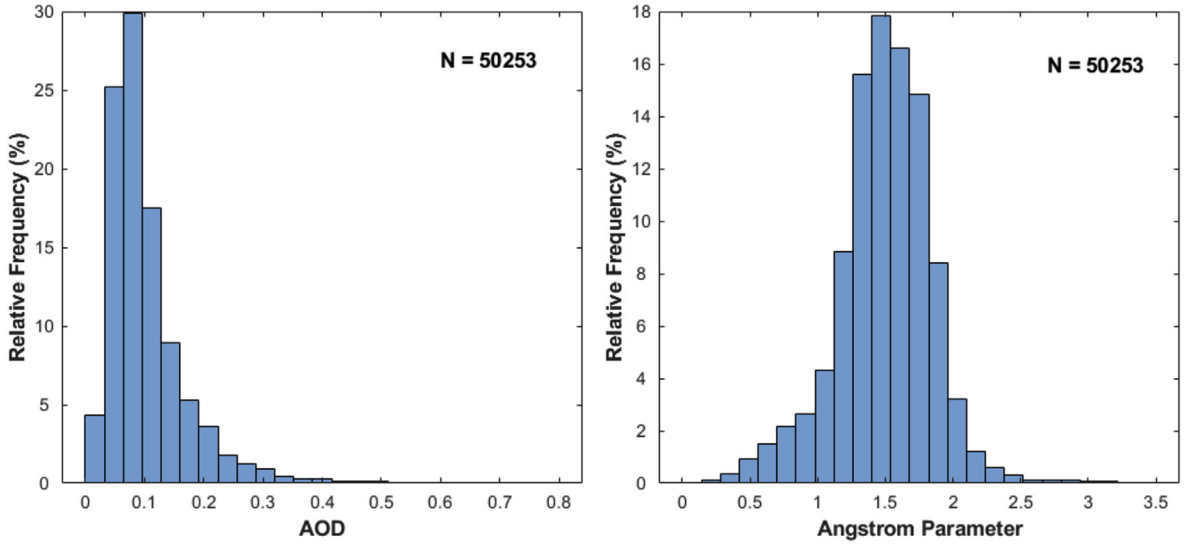

Fig. 6. Frequency distributions of AOD at 440 nm and the Angström Exponent, α (440–870 nm) for the period.

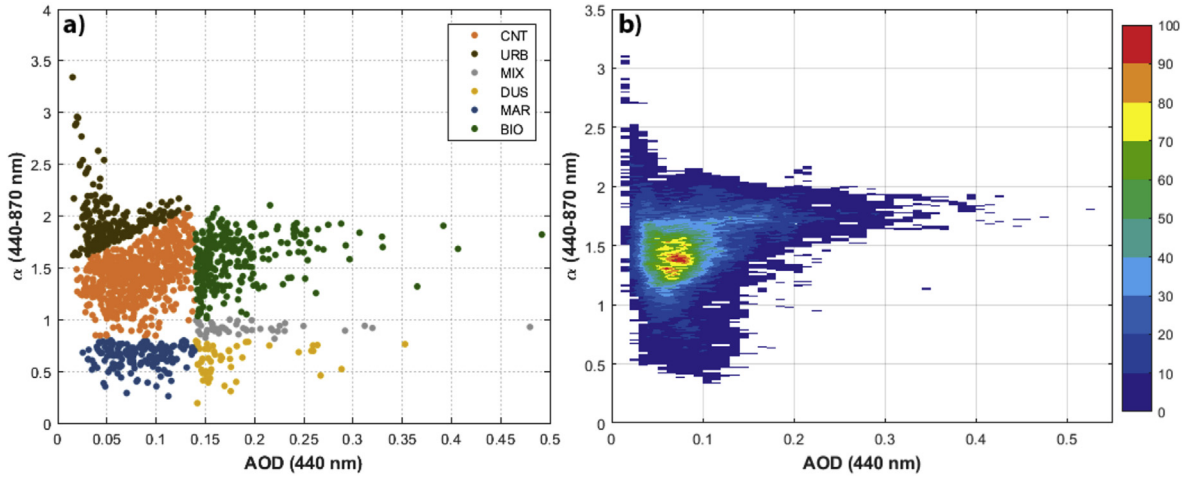

Fig. 7. Scattergram of daily means of AOD (440 nm) versus alpha (440–870 nm) (a), for aerosols classification: CNT (orange), URB (brown), MIX (gray), DUS (yellow), MAR (blue) and BIO (green). For measurements density evaluation (b) all the individual measurements made in the period between March 2015 and August 2017 were included. (For interpretation of the references to color in this figure legend, the reader is referred to the Web version of this article.)

For aerosols classification, ranges must be established to define the types of aerosols. Since the selection of a threshold between ranges is not an easy task, these limits or boundaries must be adjusted according to the specific conditions of each measurement site and its environment. An AOD vs. alpha scattergram, like the one shown in Fig. 7a, was constructed for every month. The initial thresholds were established from the existing bibliography cited above. Monthly scattergrams were used, and individual days were analyzed in order to adjust these thresholds, always taking into account the calculated air masses trajectories. The analysis carried out for the aerosol classification took into account the monthly, seasonal and annual behavior of the aerosols in the HYO. Future studies based on chemical and ionic analyses, carried out on samples acquired by particle impactors during recent campaigns, will contribute to improving the classification method.

Five aerosol types were initially considered: Continental (CNT), Dust (DUS), Maritime (MAR), Biomas (BIO) and Mixture (MIX), in accordance with studies by other authors. However, measurements with high alpha values was occasionally located over the CNT type in the scattergrams. The back trajectory analysis carried out for these cases showed that at least one of the three trajectories (500, 1500 and 3000 m) passed over the Huancayo city. A sixth aerosol type was defined then as Urban (URB). The AOD vs. alpha scattergram shown in Fig. 7a was constructed with the objective of allowing the aerosols classification and evaluating their measurement density (Fig. 7b). Likewise, the possible sources that originate the aerosols at the measurement site have been considered through the analysis of air masses addressed in the previous section. As a result of these considerations, six types of aerosols were defined (Fig. 7a) for HYO: Continental (CNT), Urban or Industrial (URB), Mixture (MIX), Dust (DUS), Maritime (MAR) and Biomas (BIO).

Fig. 7b shows the number of measurements in a two-dimensional binning, where the color scale indicates the density of the measurements by the number of data points, in intervals of 0.01 × 0.01, for both AOD and alpha. The maximum counts are enclosed in a region with $1.25 \leq \alpha \leq 1.43$ and $0.06 \leq \text{AOD} \leq 0.08$. This area corresponds to CNT type aerosols, which means the predominance of these aerosols at the measurement site with 67.1% of all types, as can be seen in Table 3. This high percent is directly related to the high percent of north and northeast air masses directions showed in Fig. 2. Trajectories from these directions move all the time over the continent and, as the CNT type, are present every month with high percentages. This type of aerosol is associated with background aerosols and the high percentage as well as its presence during all the months is indicative of the prevalence of these conditions on HYO. The CNT aerosols mainly consist of small particles with high alpha values, but in the case of AOD, this is very variable due to several reasons, but mainly due to its dependence on whether the aerosol is more or less contaminated (Hess et al., 1998; Holben et al., 2001).

Table 3
Statistics by aerosols types, including the mean values with the respective standard deviations for AOD and alpha, and the number of cases by type and frequency of occurrence.

Aerosol Types	AOD ± σ	α ± σ	Frequency	N
CNT	0.080 ± 0.028	1.419 ± 0.230	67.1	33695
URB	0.050 ± 0.025	2.016 ± 0.322	10.1	5048
MIX	0.201 ± 0.073	0.913 ± 0.058	0.3	160
DUS	0.190 ± 0.055	0.565 ± 0.169	0.5	253
MAR	0.085 ± 0.028	0.619 ± 0.134	3.8	1929
BIO	0.209 ± 0.073	1.696 ± 0.196	18.2	9168

The second more registered aerosol type at HYO is the BIO type with 18.2% (Table 3) of all aerosols measured. The BIO type, like the CNT aerosols, have high alpha values, which means that it constitutes of fine particles, although their AOD values are usually higher. The BIO type is the second source of atmospheric aerosols in HYO and the main one responsible for the increase in the AOD values at the measurement site. The BIO type aerosol modulates the monthly behavior of AOD in HYO, as can be seen in Fig. 8. As has been analyzed in the previous section, during May and August, including September, the directions of the wind from north and northeast direction predominate. But there are also trajectories originating in Brazil and arriving at HYO during a period in which a large number of biomass-burning fires occur, both in the Peruvian and Brazilian territory. With respect to the alpha values, as can be seen in Table 3, the maximum value corresponds to the URB type, which is the third aerosol type in occurrence. The maximum standard deviation for alpha corresponds to this type of aerosol.

The behavior of the BIO type describes the same monthly characteristics of the AOD monthly mean values (Fig. 5) with the maximum frequency in September, followed by August. May is the only month without the presence of BIO type but, the increase in February with respect to adjacent months, in a period when low values of AOD are registered, is also remarkable.

These aerosols are a consequence of biomass-burning from fires generated mainly in Peru but also formed as a result of forest fires in neighboring countries such as Brazil and Bolivia, although to a lesser extent (Moya et al., 2017). This transboundary transport is evident from two cases in 2016, one in August and one in September, as shown in

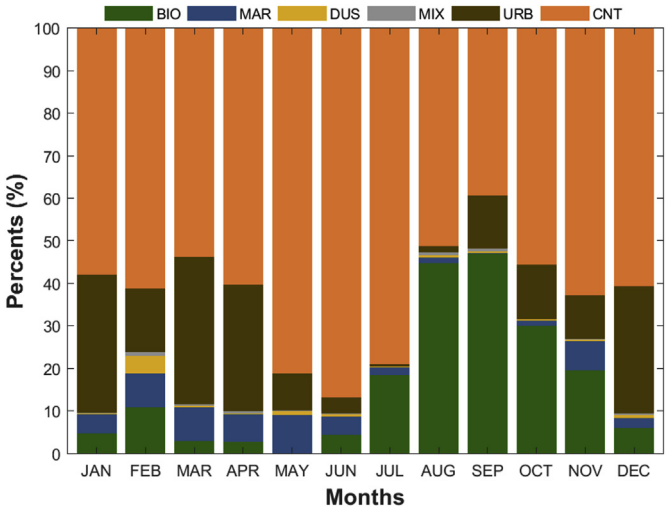

Fig. 8. Monthly percentages of presence by aerosols types in the HYO for the analyzed period.

Fig. 9. The back-trajectories (blue lines) show the transport of biomass aerosol in two cases, one from the north of Bolivia on August 5 (Fig. 9a) and another from the west of Brazil, corresponding to September 14, 2016 (Fig. 9b).

The back-trajectories were calculated using the online version of HYSPLIT model (Stein et al., 2015; Rolph et al., 2017). In both cases, the trajectories were calculated 72 h back from 21:00 UTC (time of maximum AOD value for each day). The back-trajectories were run, using Global Data Assimilation System (GDAS) as meteorological data, for different altitudes. However, around 1500 magl was where the greatest number of coincidences was found. The red dots, which signify all the fires for this day, are also shown in the figure. This information has been downloaded from the Atmospheric Composition Remote Sensing & Prediction group (ACRESP, https://www.acom.ucar.edu/acresp/). The information about fires have been provided by the Fire INventory of NCAR (FINN), where information about emissions are calculated in near-real-time using the Rapid Response MODIS fire counts (Wiedinmyer et al., 2014).

The green dots correspond to the fire points that generate the biomass aerosols type, which coincide spatially with the air masses trajectories, taking as the coincidence a criterion 10 km of radius with respect to the trajectories endpoints. In the case of aerosol transport from Bolivia (Figs. 9a), 36 coincidences were found over the territory of this country. However, it was noticeable that, over Peru, a total of 116 coincident points were detected, which means that 76% of the fires that generated biomass aerosol and were then transported to HYO originated in Peru itself. In the case of biomass aerosol transport from Brazil (Fig. 9b), where the same spatial criteria were applied, only 12 coincidences were detected. Nevertheless, the number of coincidences for Peru is also very small. Fig. 9 shows two examples for the presence of BIO aerosols on HYO as a consequence of biomass-burning fires of natural origin, but mainly generated by man. These forest fires occur mainly in Peru itself and, in the case of BIO aerosols measured in HYO, occurred both in the Andes and in the Amazon regions. In second place, there is also a contribution to the AOD registered on HYO, specifically to BIO type, due to the biomass aerosols transport by air masses from Brazil and Bolivia.

Although the biomass-burning events are frequent and are present throughout the year, the seasonality of AOD, generated by the biomass-burning, is clearly discernible from the analysis of the cases. If we consider the continuous and uninterrupted presence of this type of aerosol as the biomass-burning season for 2015, this period began on July 28 and continued until October 16, with 2747 cases and an AOD maximum value of 0.539 on September 1, at 21:28:02 UTC. For 2016, the biomass-burning season began on July 20 and ended on October 8, beginning and ending 8 days before the season in 2015. However, the number of registered cases is higher, with a total of 2909 cases, 162 more that in 2015. The absolute maximum value of AOD for all types of aerosols measured in HYO corresponds precisely to the BIO type aerosols, reaching the maximum value of 0.91 on September 14, 2016, at 11:47:46 UTC. In 2017, the biomass-burning season began on July 28, the same date as in 2015. Considering the AOD values behavior, including the Level 1.5, for the biomass-burning seasons until the present, 2016 is the year of the most intense season and with most extreme values. As has been reported by other studies using satellite and sun-photometer measurements, the intensity of the biomass-burning seasons varies from year to year (Torres et al., 2010; Pérez-Ramírez et al., 2017). However, because the AOD values corresponding to Level 2.0 of

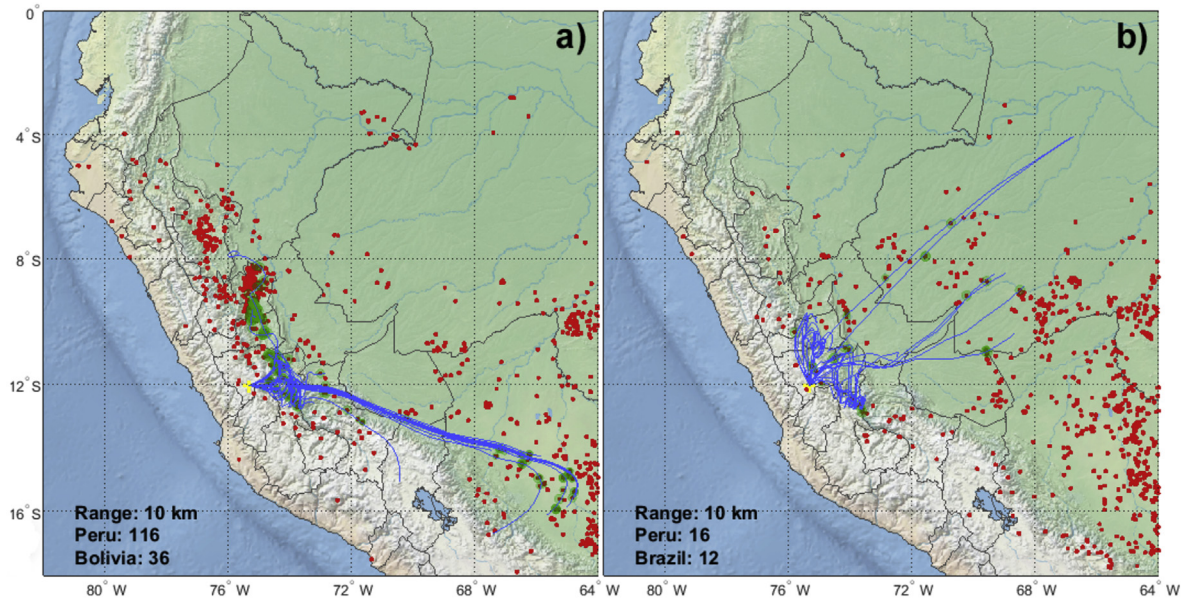

Fig. 9. Back-trajectories (blue lines) resulting from frequency analysis for August 5 (a), and September 14 (b), both cases corresponding to the year 2016 and with run start time at 21:00 UTC. Red dots represent all the active fires and green dots belong to those fires coinciding with air mass trajectories taken 10 km as spatial coincidence criteria. (For interpretation of the references to color in this figure legend, the reader is referred to the Web version of this article.)

AERONET only cover up to August 31, 2017, it is not possible to characterize the biomass-burning season during this year in the present study.

Characterizing the aerosol loading associated with forest fires during the dry season in the Amazon basin has been an issue of interest for the scientific community. For these reasons, the first large-scale deployments outside the continental United States by AERONET have been carried out in the Amazon from 1993 (Holben et al., 1998, 2001). From that moment on, seasonal campaigns were deployed in Brazil in 1994 and 1995 with the objective of studying the consequences of biomass-burning from forest fires (Holben et al., 1996; Eck et al., 1998). A recent study, which includes one of the largest AERONET records outside the United States, was conducted for the Brazilian Amazon (Schafer et al., 2008). This study divides the Amazon region into three sub-regions in order to analyze the behavior of AOD related mainly to aerosols generated by forest fires. The monthly AOD for the sub-region located west of the Brazilian Amazon and, specifically, to the Rio Branco site has the most similar behavior to the monthly averages obtained for HYO in the present study. Unlike the rest of the Brazilian AERONET sites, Rio Branco is the closest site to HYO. As in the present study, September is the month with the maximum values of AOD (440 nm) and also the month with the maximum standard deviation values. However, an important difference between both sites is that the average monthly values of AOD (above 1.2) are higher than in HYO. This Brazilian site's high values of AOD must be associated with the proximity of the measurement site to the forest fires that generate the BIO aerosol.

The AOD monthly mean values of HYO was compared with other AERONET sites located at similar altitudes. In the southern hemisphere, the La Paz site, also located in the Andes, has a very similar behavior for both, the period in which biomass-burning occurs and the AOD average values (Pérez-Ramírez et al., 2017). Differences in the AOD values, between La Paz site, located at high altitude and sites in the Amazon basin, are also significant in that study, similar to the results obtained for HYO. For the northern hemisphere, Toledano et al. (2018) reported the AOD (500 nm) monthly mean values for Mauna Loa and Izaña (3397 and 2373 masl, respectively) where, as for HYO, the AOD values are very low. In Mauna Loa, a very pristine site, the AOD annual mean barely reaches the value of 0.016; however, in the case of Izaña, this value is 0.053. In HYO, the AOD annual mean value at 500 nm is 0.083, but, at 440 nm, which is the wavelength used in this work, the mean value is 0.096. Izaña has two months with AOD mean values over 0.1, while HYO has four months exceeding this value. In the case of Izaña, this occurs during the summer season due to the Saharan dust while in HYO, the source of this increase are the biomass aerosols generated by forest fires, mainly in the Amazonia, during the winter and the beginning of spring season.

The third place corresponds to the URB aerosols that have similar characteristics to CNT aerosols, but with very high alpha values greater than 1.5 linked to very small particles. These aerosols represent 11% of all types of aerosols for the analyzed period and are related to pollution and, clearly, are a consequence of anthropogenic and industrial activities in general. The presence of this type of aerosol is concentrated during a period between mid-August 2015 and mid-June 2016. Some isolated cases took place before and after this period; however, after mid-June 2016, the number of URB aerosols cases have been very scarce, with only 12% of all cases being registered. The target of future studies will be to clarify the reasons why this type of aerosol was concentrated during this period.

The MAR type is also considered as a background aerosol and corresponds to 4% of all the aerosols measured in HYO. The main characteristics of this aerosol are its low values of alpha and AOD. The low alpha values are related to coarse particles, consistent with this aerosols' type. To date, the only existing aerosol data source to determine this type of aerosol in HYO is the CIMEL sunphotometer. Other measures will be needed to improve understanding about this type of aerosol.

Finally, with less than 1% of the total aerosols measured in the HYO in each case, we found aerosols of the MIX and DUS type. Since it is very difficult to determine the exact limit between the BIO and DUS aerosols, the MIX aerosol type is classified as a transition zone between these two types of aerosols. For this reason, this is an area where we will find a mixture of both types of aerosols.

On the other hand, the aerosol DUS has low alpha values like the aerosols type MAR and, therefore, is formed by large particles. However, this type of aerosols has high AOD values. As the BIO aerosols, they alter the background conditions. One of the possible sources of dust measured by the sunphotometer is due to the fact that the observatory is surrounded by agricultural land and since, during the periods of earth preparation, a large amount of dust is released into the atmosphere. The construction of a road in the vicinity of the observatory may also have contributed to this type of aerosols during the analyzed period. Finally, another source of dust aerosols is desert dust, which is generated by an increase of the winds in the coastal deserts of Peru, mainly in the Central Coastal Desert and in the northernmost portion of the southern region. This last zone includes some of the most important coastal deserts in Peru, such as the deserts of Ica and Paracas. The intensity of the winds in the Paracas peninsula is widely known (Gutiérrez, 2011; Sydeman, 2014), which gives rise to the name of "Paracas Winds". These powerful winds, combined with vast desert areas, give rise to the strongest dust storms where sand particles in a variety of sizes rise and, occasionally, the smallest sand particles reach the Mantaro Valley in the form of dust aerosol (Platero et al., 2018).

Optical properties

In order to show the relationship between the aerosols types and some optical properties, Fig. 10 shows the average values of Single Scattering Albedo (SSA) and the Asymmetry Factor (AF). This analysis was carried out for five of the aerosols types, according to the classification proposed in this study, excluding the MIX type. The SSA (Fig. 10a) is a measure of the absorption characteristics of the atmospheric aerosol. This variable is derived from almucantar sky radiance retrievals at four wavelengths for conditions with suitably high aerosol loading, normally greater than 0.4 at 440 nm (Dubovik et al., 2000). This is a variable correlated with the radiative forcing of the Earth's atmosphere and is defined as the amount of dispersion in relation to the total extinction in a small volume of aerosols. Values of SSA close to 0 correspond to purely absorbing particles, while values close to unity are related to purely scattering particles (Olcese et al., 2014). Given the strict conditions necessary to be accomplished to obtain SSA values, only 16 measurements of SSA are available. 10 measurements correspond to July 2016, and the rest correspond to September 2015 and 2016, with 3 measurements in each one. Only one case of the CNT type (July 30, 2016) is available; the rest of cases belong to the BIO type.

On the other hand, the AF (Fig. 10b) is a measure of the angular distribution of light scattered in the preferred scattering direction (forward or backward) due to the interaction of light with aerosols particles. In the first case (-1), the AF values range between -1 and $+1$ and the radiation is entirely backscattered; in the second ($+1$), the radiation is entirely forward scattered, and just like SSA, it depends upon the size and composition of the particles present in the atmosphere. A total of 538 measurements was involved in the analysis of AF. 269 of them correspond to the CNT type, the BIO type comes in second place with 139 cases, the URB type is in third place with 74 cases and, finally, the MAR and DUS types come with 38 and 18 cases, respectively.

The SSA (Fig. 10a) decreases with the increment of wavelengths in both types of aerosols; however, in the case of BIO type in the four wavelengths, the values are above 0.9 with the maximum value being 0.94 in 440 nm. This behavior is indicative of the presence of light absorbing particles linked to biomass-burning aerosols.

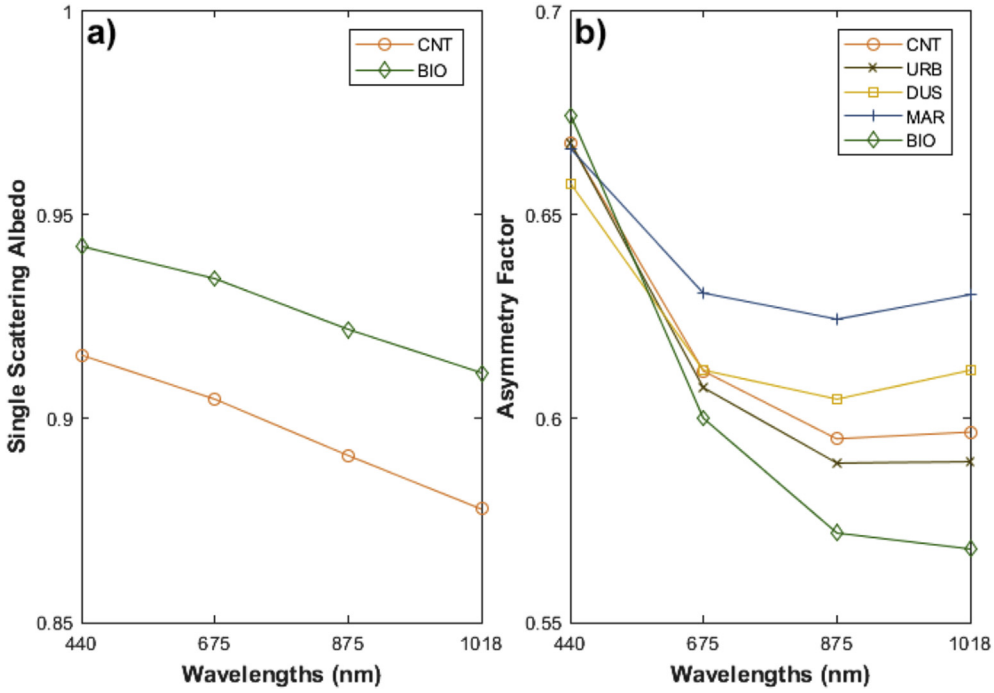

Fig. 10. The averaged values by aerosols types for Single Scattering Albedo (a) and Asymmetric Factor (b) at wavelengths 440, 675, 875 and 1018 nm.

This type of aerosols is produced by a smoldering-type combustion from woody fuel fires that burn more efficiently than grass fires (Schafer et al., 2008). In the case of the CNT type, the average SSA values are slightly lower than those of the BIO type, with a maximum at 440 nm of 0.92 and a minimum at 1018 nm less than 0.9 (0.88), which means that this type of aerosol is slightly higher absorbing than the BIO type. We can conclude from the analysis of SSA that the behavior of this variable corresponds to the aerosols classification performed in the present work.

In the case of AF (Fig. 10b), it can be noticed that the only type of aerosol that always decreases from 440 nm to 1018 nm is the BIO type. It is also noticeable that the BIO type dominates the extreme values at extreme wavelengths for all types of aerosols. The maximum value of 0.67 at 440 nm corresponds to BIO type as mentioned above, and the minimum at 1018 nm has a value of 0.57. This pronounced decrease is typical of small particles related to the generated smoke and, in this case, by the biomass-burning (Dubovik et al., 2002). On the other hand, the MAR and DUS aerosols types decrease in the visible range, between 440 and 875 nm, but increase slightly in the near infrared region (875–1018 nm). This behavior is associated with large particles such as maritime and dust aerosols with a predominant forward scattering pattern (Yu et al., 2011). The CNT and URB aerosols types decrease in the visible range but, in the infrared range, remain almost constant. While the MAR and DUS types dominate the high values of AF at 1018 nm and the BIO dominates the lower values, the CNT and URB types, which have very similar characteristics, are in the middle and very close to each other. These last two aerosols types are anthropogenic. As with the SSA analysis, the classification performed in this study responds to the optical characteristics of the aerosols, such as the asymmetry factor.

Aerosols size distribution

The aerosol volume-size distribution is derived from the irradiance measurements of the sky using the AERONET inversion algorithms (Dubovik and King, 2000). Fig. 11 shows the average values of the aerosol volume-size distribution for the analyzed period. The distribution has a bimodal character with a slight predominance of the fine

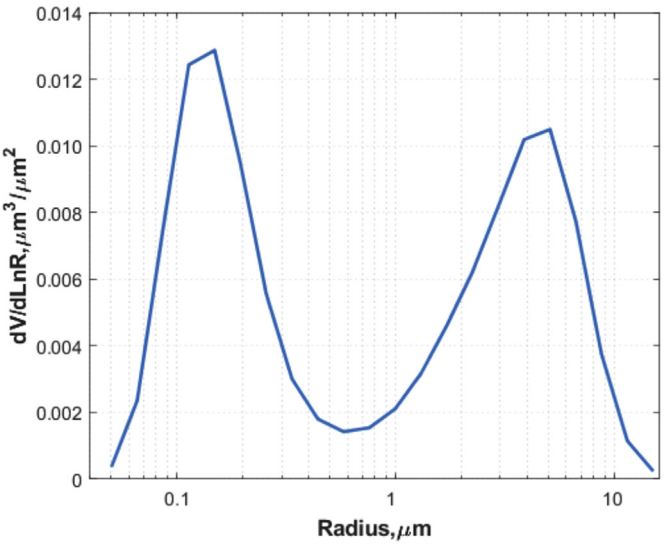

Fig. 11. Mean values of aerosol volume-size distribution for the study period.

mode corresponding to particles with a small radius. The fine mode is centered, on average, at a radius equal to 0.1482 μm, while the coarse mode (large particles) is centered at a radius of 5.0613 μm. The fine mode is linked to the CNT and URB type aerosols, all of them mainly related to human activity. BIO-type aerosols are also small particles, but in this case, they may either be related to human activity or have a natural origin. The major contribution to the fine mode corresponds to the BIO type with 60.5%, followed by the URB and CNT types with 37.5% and 2%, respectively. On the other hand, the coarse mode is linked to the aerosols types MAR and DUS, with a clear predominance of the first type (64.2%) while the DUS type reaches only 35.8%.

Average monthly values of the aerosol volume-size distribution are shown in Fig. 12. Maximum values correspond to the fine mode (radius < 0.576 μm), as observed in the previous figure. They can be found between the months of July and October with magnitudes higher than 0.02 $\mu m^3/\mu m^2$ and correspond to the fine mode, with the absolute

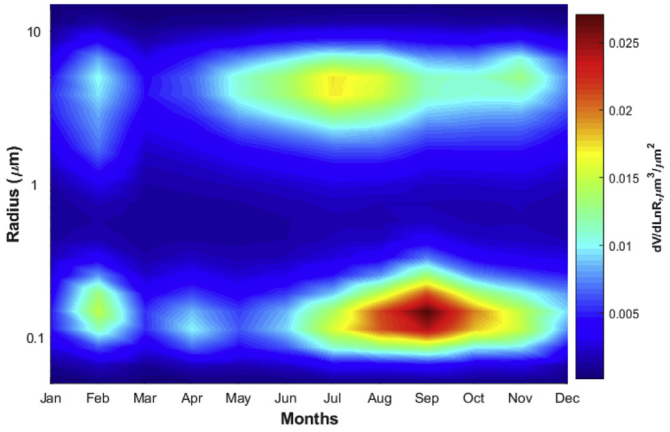

Fig. 12. Monthly mean values of aerosol volume-size distribution for the analyzed period.

maximum value centered in September, coinciding with the month in which the maximums AOD values are registered. This maximum is related to aerosols composed of small particles, which are a consequence of the biomass burning, as has previously been mentioned.

Regarding the coarse mode, the higher values are found between May and September. The coarse mode is related to the large particles linked to MAR and DUS aerosols types. The coarse mode peak appears in July; however, its minimum monthly mean alpha value correspond to May (Fig. 5b). Relatively high values in the coarse mode were also found in November. In February, there were some significant values, both in fine and coarse mode, which could explain the relatively high AOD values during this month (Fig. 5a). As can be seen in Fig. 8, these values are related to the presence of the aerosols types BIO and DUS.

The fact that maximum values of coarse mode appear in July and not in February attracts attention. The possible answer to this is related to the number of aerosol volume-size distribution measurements. The rainy season takes place mainly between December and March, with the highest accumulated in January and February. For this reason, during these months, the number of cloudy days is very high and, consequently, the number of days with almucantar measurements is very low. In fact, only four measurements are available during February, the month with the lowest percentage of size distribution measurements (0.4%). Of these four measurements days, only one of them shows a clear prevalence of the coarse mode. On the opposite side, during the winter season (June to August), the greatest number of measurements occurs (67.7%) due to the high number of days with clear sky conditions. Within this season, July is the month with the maximum number of measurements (32.4%).

4. Conclusions

The first results of aerosols characteristics, measured with a sunphotometer, for the Mantaro Valley have been shown. With an AOD mean value of 0.10 ± 0.07 for the period, it could be considered that for Huancayo Observatory, the background conditions generally prevail. The analysis of monthly means reveals that September is the month with the highest AOD values, followed by August, October and July, and in this order.

From the use of the AOD and Angström Exponent, it has been possible to classify the aerosols in six subtypes. The analysis derived from this classification has made it possible to determine that background conditions are predominant over the HYO. These background conditions are dominated, in first place, by continental aerosols with the 67.1% of all measured aerosols, followed by urban-industrial aerosols with 10.1% and, to a lesser extent, maritime aerosols (4%). An important result is the establishment of biomass-burning periods that are related to the increase of registered AOD in the HYO. These periods cover from July to October of each year and consider September as the month of the maxima. During these months, the background conditions are disrupted by the presence of biomass-burning aerosols, coinciding with the greater occurrence of forest fires, both in Peru and in neighboring countries. The arrival of biomass-burning aerosols generated by forest fires that take place in Brazil and Bolivia has also been evidenced. The biomass aerosols are the main party responsible for the increase of AOD in the Mantaro Valley and take the second place in all aerosols registered in HYO (18.2%). The dust aerosol is also responsible, but to a less extent, for the increase in AOD.

The analysis of some optical properties such as the single scattering albedo and the asymmetry factor has been used to support the performed classification. The behavior of both variables are consistent with the aerosols types. Other aerosol properties such as the volume-size distribution shows a bimodal behavior of aerosols sizes, with a very slight prevalence of the fine mode. The examination of aerosol sizes reveals the preponderance of small particles corresponding to the fine mode, related to continental, biomass and urban-industrial aerosols, in this order of influence. The months between July and October enclose the maximum values of aerosol volume-size distribution, and these correspond to the fine mode. On the other hand, large particles associated with coarse mode correspond to maritime and dust aerosols and have their greater frequency of occurrence between June and August, with the maximum in July.

The back-trajectories analysis has allowed defining two air masses patterns and two transitions months. The first pattern includes the first (January to March) and the last quarter of the year (October to December). The second pattern is constituted by the months of May to August. April is the transition month between the first part of the first pattern and the second pattern, while September is the transition month between the second pattern and the last part of the first pattern. The prevalence of wind directions between the north and the northeast is significant, with more than 71% of frequency. Air masses with these directions flow over the continent all the time, which is closely related to the CNT-type aerosols. Air masses originating in the ocean give rise to the MAR type aerosols. These same air masses, when crossing the Peruvian coastal deserts at the ground level, drag dust particles that occasionally reach the HYO and give rise to the aerosol DUS type.

Acknowledgements

This work was funded by CONCYTEC, Peru, under project MAGNET: “Attracting researchers: Strengthening the research line in physics and microphysics of the atmosphere”, agreement N° 010-2017-FONDECYT. We thank to the Inter-American Institute for Cooperation on Agriculture (IICA), Peru, for administrative support. NCEP Reanalysis data provided by he NOAA/OAR/ESRL PSD, Boulder, Colorado, USA, from their Web site at https://www.esrl.noaa.gov/psd/

Appendix A. Supplementary data

Supplementary data to this article can be found online at https://doi.org/10.1016/j.aeaoa.2019.100037.

Andrews et al., 2006, Tiwari et al., 2015

References

Aceituno, P., 1989. On the functioning of the Southern oscillation in the south American sector. Part II. Upper-air circulation. J. Clim. 2 (4), 341–355. https://doi.org/10.1175/1520-0442(1989)002<0341:OTFOTS>2.0.CO;2.

Alados-Arboledas, L., Alcantara, A., Olmo, F.J., Martinez-Lozano, J.A., Estelles, V., Cachorro, V., Silva, A.M., Horvath, H., Gangl, M., Diaz, A., 2008. Aerosol columnar properties retrieved from CIMEL radiometers during VELETA 2002. Atmos. Environ. 42, 2654–2667.

Andreae, M.O., 1993. Global distribution of fires seen from space 1993. EOS, Trans. Am. Geophys. Union 74 (12), 129–144. https://doi.org/10.1029/93EO00166.

Andrews, E., Sheridan, P., Fiebig, M., McComiskey, A., Ogren, J., Arnott, P., Covert, D., Elleman, R., Gasparini, R., Collins, D., 2006. Comparison of methods for deriving

aerosol asymmetry parameter. J. Geophys. Res. 111, 1–16.
Artaxo, P., Rizzo, L.V., Brito, J.F., Barbosa, H.M.J., Arana, A., Sena, E.T., Cirino, G.G., Bastos, W., Martine, S.T., Andreae, M.O., 2013. Atmospheric aerosols in Amazonia and land use change: from natural biogenic to biomass burning conditions. Faraday Discuss 165, 203–235. https://doi.org/10.1039/c3fd00052d.
Briceño-Zuluaga, F., Castagna, A., Rutllant, J.A., Flores-Aqueveque, V., Caquineau, S., Sifeddine, A., Velazco, F., Gutierrez, D., Cardich, J., 2017. Paracas dust storms: sources, trajectories and associated meteorological conditions. Atmos. Environ. 165, 99–110.
Chevalier, P., Pouyand, B., Suarez, W., Condom, T., 2011. Climate change threats to environment in the Tropical Andes: glaciers and water resources. Reg. Environ. Change 11 (1), 179–187. https://doi.org/10.1007/s10113-010-0177-6.
De Oliveira Alves, N., Vessoni, A.T., Quinet, A., Fortunato, R.S., Kajitani, G.S., Peixoto, M.S., De Souza Hacon, S., Artaxo, P., Saldiva, P., Martins Menck, C.F., Batistuzzo de Medeiros, S.R., 2017. Biomass burning in the Amazon region causes DNA damage and cell death in human lung cells. Nature 7 (1), 13. https://doi.org/10.1038/s41598-017-11024-3.
Dubovik, O., King, M., 2000. A flexible inversion algorithm for retrieval of aerosol optical properties from Sun and sky radiance measurements. Journal of Geophysical 105, 20673–20696.
Dubovik, O., Smirnov, A., Holben, B.N., King, M., Kaufman, Y.J., Eck, T.F., Slutsker, I., 2000. Accuracy assessmentso f aerosol optical properties retrieved from Aerosol Robotic Network (AERONET) Sun and sky radiance measurements. Journal of Gepphysucal Research 105 (D8), 9791–9806. https://doi.org/10.1029/2000JD900040.
Dubovik, O., Holben, B.N., Eck, T.F., Smirnov, A., Kaufman, Y.J., King, M.D., Tanré, D., Slutsker, I., 2002. Variability of absorption and optical properties of key aerosol types observed in worldwide locations. J. Atmos. Sci. 59 (3), 590–608 doi:1520-0469(2002)059 < 0590:VOAAOP > 2.0.CO;2.
Dubovik, O., Sinyuk, A., Lapyonok, T., Holben, B.N., Mishchenko, M., Yang, P., Eck, T.F., Volten, H., Muoz, O., Veihelmann, B., 2006. Application of spheroid models to account for aerosol particle nonsphericity in remote sensing of desert dust. J. Geophys. Res. 104, 1–34.
Dumka, U., Moorthy, K., Satheesh, S., Sagar, R., Pant, P., 2008. Short-period modulations in aerosol optical depths over the central Himalayas: role of mesoscale processes. Journal of Applied Meteorology and Climatology 47, 1467–1475.
Dyurgerov, M.B., Meier, M.F., 2005. Glaciers and the Changing Earth System: a 2004 Snapshot. Institute of Arctic and Alpine Research Occasional Paper. University of Colorado, Boulder, Colorado, USA.
D'Almeida, G.A., Koepke, P., Shettle, E.P., 1991. Atmospheric Aerosol: Global Climatology and Radiative Characteristics. A Deepak Publishing Co, Hampton, Virginia, USA.
Eck, T.F., Holben, B.N., Slutsker, I., Setzer, A., 1998. Measurements of irradiance attenuation and estimation of aerosol single scattering albedo for biomass burning aerosols in Amazonia. J. Geophys. Res. 103 (D24), 31,865–31,878.
Eck, T.F., Holben, B.N., Reud, J.S., Dubovik, O., Siminov, A., O'Neill, N.T., Slutsker, I., Kinne, S., 1999. Wavelength dependence of the optical depth of biomass burning, urban and desert dust aerosols. J. Geophys. Res. 104, 333–349.
Escobar, D.F., 1993. Evaluación climatológica y sinóptica del fenómeno de vientos Paracas. Lima, Perú. Tesis para optar el título de Ingeniero Meteorológico. Universidad Nacional Agraria La Molina 62 pp. https://es.scribd.com/doc/8839005/.
Flanner, M.G., Zender, C.S., Randerson, J.T., Rasch, P.J., 2007. Present-day climate forcing and response from black carbon in snow. J. Geophys. Res. 112 (D11202), D11202. https://doi.org/10.1029/2006JD008003.
Garreaud, R., 1999. Multi-scale analysis of the summertime precipitation over the central Andes. Mon. Weather Rev. 127, 901–921.
Garreaud, R., 2009. The Andes climate and weather. Adv. Geosci. 22, 3–11.
Garreaud, R., Vuille, M., Clement, A.C., 2003. The climate of the Altiplano: observed current conditions and mechanisms of past changes. Palaeogeogr. Palaeoclimatol. Palaeoecol. 194, 5–22.
Gobbi, G.P., Kaufman, Y.J., Koren, I., Eck, T.F., 2007. Classification of aerosol properties derived from AERONET direct sun data. Atmos. Chem. Phys. 7, 453–458.
Gutiérrez, D.I., 2011. Coastal cooling and increased productivity in the main upwelling zone off Peru since the mid-twentieth century. Geophys. Res. Lett. 38, 1–6.
Hess, M., Koepke, P., Schult, I., 1998. Optical properties of aerosols and clouds: the software package OPAC. Bulletin of the American Metreological Society 79 (5), 831–844 doi:1520-0477(1998)079%3C0831:OPOAAC%3E2.0.CO;2.
Holben, B.N., Setzer, A., Eck, T.F., Pereira, A., Slutsker, I., 1996. Effect of dry-season biomass burning on Amazon basin aerosol concentrations and optical properties, 1992–1994. J. Geophys. Res. 101 (D14), 19,465–19,482.
Holben, B.N., Eck, T.F., Slutsker, I., Tanre, D., Buis, J.P., Setzer, A., Vermote, E.F., Reagan, J.A., Kaufman, Y.J., Nakajima, T., Lavenu, F., Jankowiak, I., Smirnov, A., 1998. AERONET – a federated instrument network and data archive for aerosol characterization. Rem. Sens. Environ. 66, 1–16.
Holben, B.N., Tanré, D., Smirnov, A., Eck, T.F., Slutsker, I., Abuhassan, N., Newcomb, W.W., Schafer, J.S., Chatenet, B., Lavenu, F., Kaufman, Y.J., Van Castle, J., Setser, A., Markham, B., Clark, B., Frouin, R., Halthore, R., Karneli, A., O'Neill, N.T., Pietras, C., Pinker, R.T., Voss, K., Zibordi, G., 2001. An emerging ground-based aerosol climatology: aerosol optical depth from AERONET. J. Geophys. Res. 106 (D11), 12067–12097. https://doi.org/10.1029/2001JD900014.
Holben, B.N., Eck, T.F., Slutsker, I., Smirnov, A., Sinyuk, A., Schafer, J., Giles, D., Dubovik, O., 2006. Aeronet's Version 2.0 quality assurance criteria. Proc. SPIE 64080Q.
IPCC, 2007. Climate Change 2007: the Physical Science Basis. Contribution of Working Group I to the Fourth Assessment. Cambridge University Press, Cambridge Recuperado el 15 de 06 de 2015, de IPCC.
IPCC, 2013. Climate Change 2013: the Physical Science Basis. Contribution of Working Group I to the Fifth Assessment Report of the Intergovernmental Panel on Climate Change. Cambridge. Cambridge University Press, United Kingdom and New York, NY, USA.
Jacobson, M.Z., 2004. Climate response of fossil fuel and biofuel soot, accounting for soot's feedback to snow and sea ice albedo and emissivity. J. Geophys. Res. 109 (D21201), 15. https://doi.org/10.1029/2004JD004945.
Kalnay, E., Kanamitsu, M., Kistler, R., Collins, W., Deaven, D., Gandin, L., Iredell, M., Saha, S., White, G., Woollen, J., Zhu, Y., Chelliah, M., Ebisuzaki, W., Higgins, W., Janowiak, J., Mo, K.C., Ropelewski, C., Wang, J., Leetmaa, A., Reynolds, R., Jenne, R., Joseph, D., 1996. The NCEP/NCAR 40-year reanalysis project. Bull. Am. Meteorol. Soc. 77 (3), 437–471. https://doi.org/10.1175/1520-0477(1996)077 < 0437:tnyrp > 2.0.co;2.
Lenters, J.D., Cook, K.H., 1997. On the origin of the Bolivian High and related circulation features of the South American climate. J. Atmos. Sci. 54, 656–677.
Mishra, A.K., Lehahn, Y., Rudich, Y., Koren, I., 2015. Co-variability of smoke and fire in the Amazon basin. Atmos. Environ. 109, 97–104. https://doi.org/10.1016/j.atmosenv.2015.03.007.
Moya, A.S., Estevan, R., Yuli, R.A., 2017. Determinación de la presencia de partículas PM10 en Perú, producidas por quema de biomasa con ayuda de modelos numéricos. RICA 33 (1).
Olcese, L.E., Palancar, G.G., Toselli, B.M., 2014. AerosolopticalpropertiesincentralArgentina. J. Aerosol Sci. 68, 25–37. https://doi.org/10.1016/j.jaerosci.2013.11.003.
Otero, L., Ristori, P., Holben, B., Quel, E., 2006. Espesor óptico de aerosoles durante el año 2002 para diez estaciones pertenecientes a la red AERONET – NASA. Opt. Pura Apl. 39 (4), 355–364.
Pérez-Ramírez, D., Andrade, M., Eck, T., Stein, A., O'Neill, N., Lyamani, H., Gassó, S., Whiteman, D.N., Veselovskii, I., Velarde, F., Alados-Arboledas, L., 2017. Multi year aerosol characterization in the tropical Andes and in adjacent Amazonia using AERONET measurements. Atmos. Environ. 17https://doi.org/10.1016/j.atmosenv.2017.07.037. 1352-2310.
Platero, I.Y., Estevan, R., Moya, A.S., Yuli, R.A., 2018. Determining the desert dust aerosol presence in the Mantaro Valley, Peru (In Spanish). Opt. Pura Apl. 51 (3), 1–14. https://doi.org/10.7149/OPA.51.3.50023. 50023.
Quijano, J.J., 2013. Estudio numérico y observacional de la dinámica de Viento Paracas, asociado al transporte eólico hacia el océano frente a la costa de Ica-Perú. MSc Thesis. Universidad Peruana Cayetano Heredia, Lima - Perú 151 pp. http://www.met.igp.gob.pe/publicaciones/2013/JQuijano_tesisMSc.pdf.
Rolph, G., Stein, A., Stunder, B., 2017. Real-time environmental applications and display sYstem: READY. Environ. Model. Softw 95, 210–228. https://doi.org/10.1016/j.envsoft.2017.06.025.
Russell, P.B., Bergstrom, R.W., Shinozuka, Y., Clarke, A.D., DeCarlo, P.F., Jimenez, J.L., M Livingston, J., Redemann, J., Dubovik, O., Strawa, A., 2010. Absorption Angstrom Exponent in AERONET and related data as an indicator of aerosol composition. Atmos. Chem. Phys. 10, 1155–1169.
Schafer, J.S., Eck, T.F., Holben, B.N., Artaxo, P., Duarte, A.F., 2008. Characterization of the optical properties of atmospheric aerosols in Amazônia from long-term AERONET monitoring (1993–1995 and 1999–2006). J. Geophys. Res. 113 (D04204). https://doi.org/10.1029/2007JD009319.
Silva, Y., Takahashi, K., Chávez, R., 2008. Dry and wet rainy seasons in the Mantaro river basin (Central Peruvian Andes). Adv. Geosci. 14, 261–264.
Smirnov, A., Holben, B.N., Eck, T.F., Dubovik, O., Slutsker, I., 2000. Cloud screening and quality control algorithms for the AERONET database. Rem. Sens. Environ. 73, 337–349.
Stein, A.F., Draxler, R.R., Rolph, G.D., Stunder, B.J., Cohen, M.D., Ngan, F., 2015. NOAA's HYSPLIT atmospheric transport and dispersion modeling system. Bull. Am. Meteorol. Soc. 96, 2059–2077. https://doi.org/10.1175/BAMS-D-14-00110.1.
Suárez, L., Castillo, L., Marín, M., Carrillo, G., Rimac, L., Pomalaya, J., Menacho, R., 2006. Estudios de la variación estacional de ozono troposferico y aerosoles del Perú relacionado a las quemas de vegetación en la Amazonía. Mosaico Científico 3 (3), 36–41.
Sydeman, W.J.-R., 2014. Climate change and wind intensification in coastal upwelling ecosystems. Sci. New York 345, 77–80.
Tiwari, S., Srivastava, A.K., Singh, A.K., Singh, S., 2015. Identification of aerosol types over Indo-Gangetic Basin: implications to optical properties and associated radiative forcing. Environ. Sci. Pollut. Control Ser. 22, 12246–12260.
Toledano, C., Cachorro, V.E., Berjon, A., de Frutos, A.M., Sorribas, M., de la Morena, B.A., Goloub, P., 2007. Aerosol optical depth and Ångström exponent climatology at El Arenosillo AERONET site (Huelva, Spain). Q. J. R. Meteorol. Soc. 133, 795–807. https://doi.org/10.1002/qj.54.
Toledano, C., González, R., Fuertes, D., Cuevas, E., Eck, T.F., Kazadzis, S., Kouremeti, N., Gröbner, J., Goloub, P., Blarel, L., Román, R., Barreto, Á., Berjón, A., Holben, B.N., Cachorro, V.E., 2018. Assessment of sun photometer langley calibration at the high-elevation sites Mauna Loa and Izaña. Atmos. Chem. Phys. 18 (19), 14555–14567. https://doi.org/10.5194/acp-18-14555-2018.
Torres, O., Chen, Z., Jethva, H., Ahn, C., Freitas, S., Barthia, P., 2010. OMI and MODIS observations of the anomalous 2008-2009 Southern Hemisphere biomass burning seasons. Atmos. Chem. Phys. 10, 3505–3513.
Vergaz, R., Cachorro, V.E., Frutos, A.M., Vilaplana, J.M., Morena, B.A., 2005. Columnar characteristics of aerosols by spectroradiometer measurements in the maritime area of the Cadiz Gulf (Spain). Int. J. Climatol. 25, 1781–1804.
Verma, S., Prakash, D., Ricaud, P., Payra, S., Attié, J.-L., Soni, M., 2015. A new classification of aerosol sources and types as measured over Jaipur, India. Aerosol and Air Quality Research 15, 985–993.

Vivanco, S., 2014. Variabilidad Temporal de Aerosoles Atmosféricos en Huancayo. Apuntes de Ciencia y Sociedad 4 (1), 57–68. dx.doi.org/10.18259/acs.2014006.
Vuille, M., 1999. Atmospheric circulation over the Bolivian Altiplano during dry and wet periods and extreme phases of the Southern Oscillation. Int. J. Climatol. 19, 1579–1600.
Vuille, M., Keimig, F., 2004. Interannual variability of summertime convective cloudiness and precipitation in the central Andes derived from ISCCP-B3 data. J. Clim. 17, 3334–3348.
Vuille, M., Bradley, R.S., Keimig, F., 2000. Interannual climate variability in the Central Andes and its relation to tropical Pacific and Atlantic forcing. J. Geophys. Res. 105, 12,447–12,460.
Vuille, M., Kaser, G., Juen, I., 2008. Glacier mass balance variability in the Cordillera Blanca, Peru and its relationship with climate and the large-scale circulation. Glob. Planet. Chang. 62, 14–28.
Warren, S.G., 1984. Impurities in snow: effects on albedo and snowmelt. Ann. Glaciol. 5, 177–179.
Warren, S.G., Wiscombe, W., 1980. A model for the spectral albedo of snow. II: snow containing atmospheric aerosols. J. Atmos. Sci. 37, 2734–2745.
Wiedinmyer, C., Yokelson, R.J., Gullett, B.K., 2014. Global emissions of trace gases, particulate matter, and hazardous air pollutants from open burning of domestic waste. Environ. Sci. Technol. 48 (16), 9523–9530. https://doi.org/10.1021/es502250z.
Yu, X., Zhu, B., Yin, Y., Yang, J., Li, Y., Bu, X., 2011. A comparative analysis of aerosol properties in dust and haze-fog days in a Chinese urban region. Atmos. Res. 99, 241–247. https://doi.org/10.1016/j.atmosres.2010.10.015.

Update

Atmospheric Environment: X

Volume 8, Issue , December 2020, Page

DOI: https://doi.org/10.1016/j.aeaoa.2020.100087

ATMOSPHERIC ENVIRONMENT: X 8 (2020) 100087

Contents lists available at ScienceDirect

Atmospheric Environment: X

journal homepage: http://www.journals.elsevier.com/atmospheric-environment-x

Erratum regarding previous published articles

Owing to a Publisher error Declaration/Conflict of Interest statements were not included in the published versions of the following articles, that appeared in previous issues of *Atmospheric Environment:*

The authors declare that they have no known competing financial interests or personal relationships that could have appeared to influence the work reported in this paper.

1. On the spatial representativeness of NOX and PM10 monitoring-sites in Paris, France, Volume 1, January 2019, 100010,10.1016/j.aeaoa. 2019.100010.

Declaration of competing interest

The authors declare that they have no known competing financial interests or personal relationships that could have appeared to influence the work reported in this paper.

2. NOX and PM10 Bayesian concentration estimates using high-resolution numerical simulations and ground measurements over Paris, France, Volume 3, July 2019, 10003810.1016/j.aeaoa. 2019.100038.

Declaration of competing interest

The Authors wish to confirm that there are no known conflicts of interest associated with this publication and there has been no significant financial support for this work that could have influenced its outcome.

3. Measured and Modelled Ozone Photochemical Production in the Baltimore-Washington Airshed, Volume 2, April 2019, 10001710.1016/j.aeaoa. 2019.100017.

Declaration of competing interest

The authors declare that they have no known competing financial interests or personal relationships that could have appeared to influence the work reported in this paper.

4. First two and a half years of aerosol measurements with an AERONET sunphotometer at the Huancayo Observatory, Peru, Volume 3, July 2019, 10003710.1016/j.aeaoa. 2019.100037.

Declaration of competing interest

The authors declare that they have no known competing financial interests or personal relationships that could have appeared to influence the work reported in this paper.

5. NO2 hotspots: are we measuring in the right places? Volume 2, April 2019, 10002510.1016/j.aeaoa. 2019.100025.

Declaration of competing interest

The authors declare that they have no known competing financial interests or personal relationships that could have appeared to influence the work reported in this paper.

6. Observation of column-averaged molar mixing ratios of carbon dioxide in Tokyo, Volume 2, April 2019, 10002210.1016/j.aeaoa. 2019.100022.

Declaration of competing interest

The authors declare that they have no known competing financial interests or personal relationships that could have appeared to influence the work reported in this paper.

7. Evaluation of an operational air quality model using large-eddy simulation, Volume 3, July 2019, 100041,10.1016/j.aeaoa. 2019.100041.

Declaration of competing interest

The authors declare that they have no known competing financial interests or personal relationships that could have appeared to influence the work reported in this paper.

8. Comparisons of the vertical distributions of aerosols in the CALIPSO and GEOS-Chem datasets in China, Volume 3, July 2019, 100036,10.1016/j.aeaoa. 2019.100036.

Declaration of competing interest

The authors declare that they have no known competing financial interests or personal relationships that could have appeared to influence the work reported in this paper.

9. A trend analysis approach for air quality network data, Volume 2,

DOIs of original article: https://doi.org/10.1016/j.aeaoa.2019.100036, https://doi.org/10.1016/j.aeaoa.2019.100041, https://doi.org/10.1016/j.aeaoa.2019.100038, https://doi.org/10.1016/j.aeaoa.2019.100025, https://doi.org/10.1016/j.aeaoa.2019.100037, https://doi.org/10.1016/j.aeaoa.2019.100030, https://doi.org/10.1016/j.aeaoa.2019.100032, https://doi.org/10.1016/j.aeaoa.2019.100010, https://doi.org/10.1016/j.aeaoa.2019.100017, https://doi.org/10.1016/j.aeaoa.2019.100039, https://doi.org/10.1016/j.aeaoa.2019.100022.

https://doi.org/10.1016/j.aeaoa.2020.100087

Available online 10 September 2020

April 2019, 100030,10.1016/j.aeaoa. 2019.100030.

Declaration of competing interest

The authors declare that they have no known competing financial interests or personal relationships that could have appeared to influence the work reported in this paper.

10. Long-term health impact assessment of total PM2.5 in Europe during the 1990–2015 period, Volume 3, July 2019, 100032,10.1016/j.aeaoa. 2019.100032.

Declaration of competing interest

The authors declare that they have no known competing financial interests or personal relationships that could have appeared to influence the work reported in this paper.

11. Emission Influences on Air Pollutant Concentrations in New York State: II. PM2.5 Organic and Elemental Carbon Constituents, Volume 3, July 2019, 100039,10.1016/j.aeaoa. 2019.100039.

Declaration of competing interest

The authors declare that they have no known competing financial interests or personal relationships that could have appeared to influence the work reported in this paper.